

SAG therapy restores bone growth and reduces enchondroma incidence in a model of skeletal chondrodysplasias caused by *Ihh* deficiency

Xinhua Li,^{1,2,3} Shuting Yang,¹ Zahra Chinipardaz,^{1,4} Eiki Koyama,⁵ and Shuying Yang^{1,6,7}

¹Department of Basic and Translational Sciences, School of Dental Medicine, University of Pennsylvania, Philadelphia, PA 19104, USA; ²Department of Orthopedics, Shanghai General Hospital, Shanghai Jiao Tong University School of Medicine, Shanghai 200080, China; ³Department of Spinal Surgery, East Hospital, Tongji University, School of Medicine, Shanghai 200120, China; ⁴Department of Periodontics, School of Dental Medicine, University of Pennsylvania, Philadelphia, PA 19104, USA; ⁵Division of Orthopedic Surgery, Department of Surgery, The Children's Hospital of Philadelphia, Philadelphia, PA 19104, USA; ⁶Center for Innovation & Precision Dentistry, School of Dental Medicine, School of Engineering and Applied Sciences, University of Pennsylvania, PA 19104, USA; ⁷The Penn Center for Musculoskeletal Disorders, School of Medicine, University of Pennsylvania, Philadelphia, PA 19104, USA

Inactivation mutations in the Indian hedgehog (*Ihh*) gene in humans cause numerous skeletal chondrodysplasias, including acrocapitofemoral dysplasia, brachydactyly type A1, and human short stature. The lack of an appropriate human-relevant model to accurately represent these chondrodysplasias has hampered the identification of clinically effective treatments. Here, we established a mouse model of human skeletal dysplasia induced by *Ihh* gene mutations via ablation of *Ihh* in Aggrecan-positive (*Acan*⁺) cells using Aggrecan (*Acan*)-creERT transgenic mice. Smoothen agonist (SAG) promoted Hh activity and rescued chondrocyte proliferation and differentiation by stimulating smoothed trafficking to the cilium in *Ihh*-silenced cells. SAG treatment corrected mouse stature and significantly decreased mortality without evidence of toxicity. Moreover, *Ihh* ablation in *Acan*⁺ cells produced enchondroma-like tissues near the growth plates that were significantly reduced by SAG treatment. These results demonstrated that SAG effectively treats skeletal dysplasia caused by *Ihh* gene mutations in a mouse model, suggesting that SAG may represent a potential drug for the treatment of these diseases and/or enchondromas.

INTRODUCTION

Inactivation mutations in the Indian hedgehog (*Ihh*) gene in humans cause numerous skeletal chondrodysplasias, including acrocapitofemoral dysplasia,¹ brachydactyly type A1,^{2,3} and human short stature.⁴ Skeletal chondrodysplasias caused by *Ihh* gene inactivation mutations have been reported to be among the most common forms of idiopathic short stature and are clinically characterized by variable degrees of short stature, short limbs, brachydactyly, and narrow thorax with pectus deformities.^{2–5} Currently, there is no effective treatment for these diseases. Although human growth hormone has been used to treat these diseases, little evidence has confirmed the effectiveness of such treatments^{4,6} due to the lack of an ideal animal model for testing the efficacy of therapeutic strategies and drugs. *Ihh* null mice are embryonic lethal at the early developmental stage, when *Ihh* expression

is normally detected in the visceral endoderm.^{7–10} Therefore, the development of an animal model to accurately represent *Ihh* gene mutation-related dysplasia is essential for drug development and repurposing.

An elevated level of Hh signaling has been reported to contribute to various stages of carcinogenesis, including enchondroma and chondrosarcoma.^{11,12} Although preclinical data on the therapeutic role of Hh antagonists in chondrosarcoma are promising, the clinical data of a phase II trial in patients have been discouraging.^{13,14} In addition, it was recently reported that Hh signaling is downregulated in several cancers and that its restoration restrains tumor growth.¹⁵ This discrepancy suggests that the relationship between *Ihh* levels and enchondroma/chondrosarcoma development is complicated.

Ihh binds to the membrane receptor protein Patched (*Ptc*) to relieve the inhibition of the membrane protein smoothed (*Smo*), which allows *Smo* to enter the cilium and activate Gli transcription factors, thus regulating target gene expression.^{16–18} Smoothen agonist (SAG) is a derivative of chlorobenzothiothiophene that binds and activates *Smo*, thus upregulating the canonical *Ihh* pathway. Recently, SAG has been reported to successfully correct structural and cognitive deficits in a Down syndrome mouse model and prevent glucocorticoid-induced neonatal cerebellar injury by activating Hh signaling.^{19,20} However, the preclinical therapeutic effect of SAG in animal models of *Ihh* gene mutation-related dysplasia has not yet been explored.

Because ablating *Ihh* in type II collagen-cre (*Col2-cre*) mice at the embryonic stage causes embryonic lethality, we chose to delete the *Ihh*

Received 17 March 2021; accepted 24 September 2021;
<https://doi.org/10.1016/j.omtm.2021.09.015>.

Correspondence: Shuying Yang, Department of Basic and Translational Science, School of Dental Medicine, University of Pennsylvania, 240 South 40th Street, Levy 437, Philadelphia, PA 19104-6030.

E-mail: shuyingy@upenn.edu



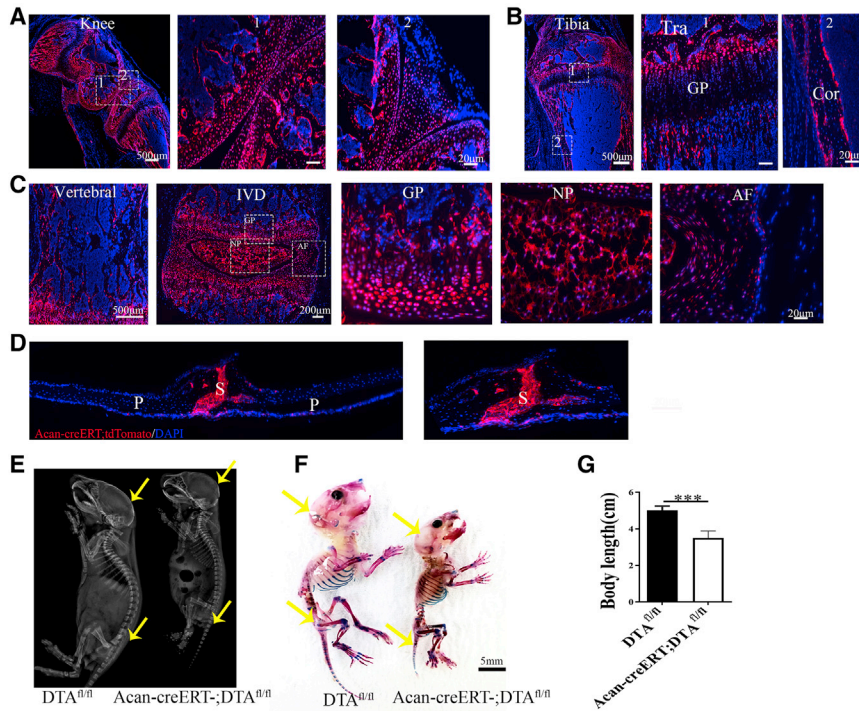


Figure 1. Acan⁺ progenitors are major contributors to postnatal skeletal development

(A–D) Acan-creERT;tdTomato mice were administered tamoxifen (TM) at P3 and harvested at P30. (A) Representative fluorescent images from frozen sections of the knee (left panel), articular cartilage (middle panel), and meniscus (right panel). (B) Representative fluorescent images from frozen sections of the tibia, growth plate, trabecular bone, and cortical bone (GP, growth plate; Tra, trabecular bone; Cor, cortical bone). (C) Representative fluorescent images from frozen sections of the vertebral bone and IVD (IVD, intervertebral disc; NP, nucleus pulposus, AF, annulus fibrosus). (D) Representative confocal images showing the lambdoid suture of the skull (P, parietal bone; S, suture). Red: tdTomato; blue: DAPI. (E–G) Acan-creERT;DTA^{fl/fl} or DTA^{fl/fl} littermates were treated with TM once daily for 2 consecutive days starting at P3 and harvested at P10. (E) Representative X-ray of DTA^{fl/fl} and Acan-creERT;DTA^{fl/fl} mice at P10. Arrow depicts the skull and spine development defects. (F) Representative images of mice that were double stained with alizarin red/Alcian blue in DTA^{fl/fl} and Acan-creERT;DTA^{fl/fl} mice at P10. Arrow depicts the skull and spine development defects. Bar is 5mm. (G) Quantity analysis showed the average body length decreased from 4.9 cm in the Acan-creERT group to 3.5 cm in the Acan-creERT;DTA^{fl/fl} mice at P10. Six mice evaluated in each group.

gene at the postnatal stage.¹⁰ It was reported that Aggrecan-creERT marks the largest number of skeletal stem cells in mice, and we generated Acan-creERT;Ihh^{fl/fl} mice in which Ihh was ablated from Acan+ skeletal stem cells by induction with tamoxifen (TM) in this study.²¹ The phenotype of these mice highly resembled that of the human skeletal dysplasia caused by Ihh mutations. In addition, this mouse model manifested multiple enchondroma-like lesions around growth plates. Our results showed for the first time that SAG rescues the proliferation and differentiation of Ihh-silenced chondrocytes by stimulating smoothed trafficking onto cilia to restore Hh activity in Ihh-silenced cells *in vitro*. SAG also corrects dwarfism and other Ihh mutation-related phenotypes and reduces enchondroma-like tissue in Ihh-deficient mice. Our data demonstrated that SAG may represent a promising treatment modality for the Ihh mutation phenotype and other disorders related to hypoactivation of Hh signaling.

RESULTS

Acan⁺ progenitors are major contributors to postnatal skeletal development

To test the efficiency and specificity of Cre recombination, we crossed Acan-creERT mice with R26-tdTomato reporter mice, which express red fluorescence upon cre activation. Acan-creERT;tdTomato mice were intraperitoneally (i.p.) injected with a single dose of TM (75 mg/kg) at postnatal day (P) 3 and then harvested at P30. We found that most of the cells in the articular cartilage (Figure 1A), growth plate, trabecular and cortical bone of the long bone (Figure 1B), and vertebral spine and intervertebral disc (IVD) (Figure 1C) were tdTomato-positive (tdTomato+) at P30. In addition, the major-

ity of cells in the suture of the skull bone also displayed strong tdTomato+ signaling (Figure 1D).

To further characterize the function of Acan+ cells in mouse postnatal skeletal development, mice bearing a diphtheria toxin (DTA) transgene downstream of a floxed stop codon (DTA^{fl/fl}) were crossed with Acan-creERT transgenic mice to ablate Acan+ cells. Acan-creERT littermates served as the control (wild-type group). Specifically, TM was i.p. injected into either Acan-creERT;DTA^{fl/fl} or Acan-creERT mice at P3. By 1 week following TM injection, all Acan-creERT;DTA^{fl/fl} mice died spontaneously (20/20). Skeletal X-ray radiographs and alizarin red/Alcian blue staining analysis showed dwarfism and skeletal development defect phenotypes in Acan-creERT;DTA^{fl/fl} mice (Figures 1E and 1F). Quantity analysis showed the average body length decreased from 4.9 cm in the Acan-creERT group to 3.5 cm in the Acan-creERT;DTA^{fl/fl} mice at P10 (Figure 1G). Thus, these results revealed that Acan+ progenitors are major contributors to postnatal skeletal development.

Ablation of Ihh in Acan⁺ progenitors causes skeletal chondrodysplasia mimicking the human Ihh gene mutation phenotype

To determine whether postnatal ablation of Ihh in Acan+ cells causes a human Ihh gene mutation-like phenotype in mice, Ihh^{fl/fl} mice were mated with Acan-creERT transgenic mice. Acan-creERT;Ihh^{fl/fl} mice were born according to the Mendelian ratio and did not show any phenotypic abnormalities. Ihh^{fl/fl} and Acan-creERT;Ihh^{fl/fl} mice were i.p. administered TM at P3 and P5 and harvested at P30. The

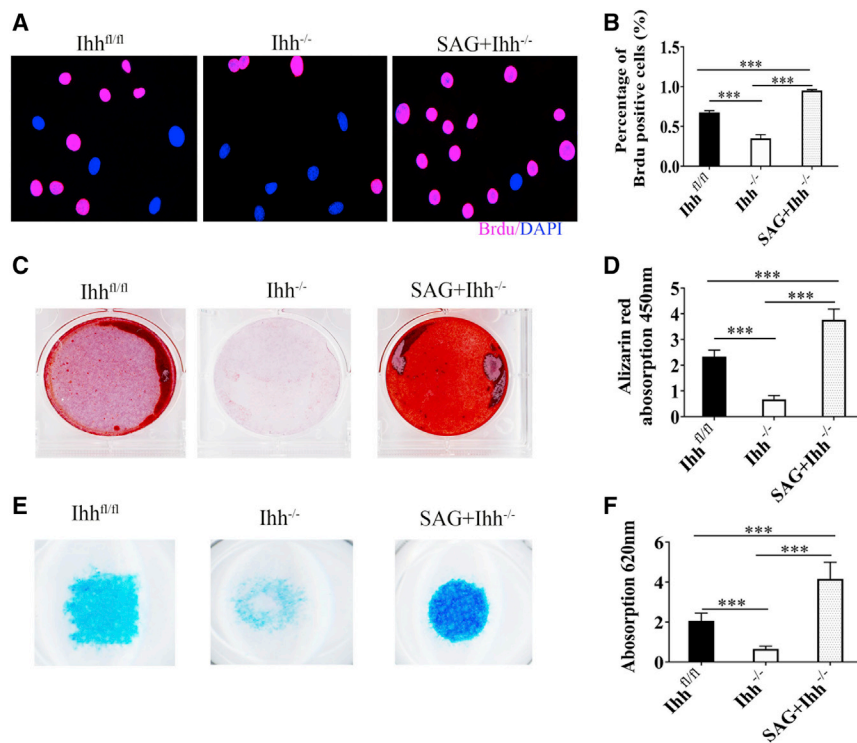


Figure 2. SAG rescues deficient chondrocyte proliferation and differentiation in Ihh silenced cells

(A) Immunofluorescent staining for BrdU and DAPI showing the proliferative chondrocyte from wild-type, Ihh-deficient, and Ihh-deficient with SAG treatment groups. Red: tdTomato; blue: DAPI. (B) Quantitative measurement of BrdU⁺ cells in (A) (n = 3, triplicates per group). (C) Alizarin red staining for osteogenesis ability of chondrocytes from wild-type, Ihh-deficient, and Ihh-deficient with SAG treatment groups. (D) Quantitative measurement of osteogenesis differentiation ability in (C) (n = 3, triplicates per group). (E) Alcian blue staining for chondrogenesis differentiation ability of chondrocyte from wild-type, Ihh-deficient, and Ihh-deficient with SAG treatment groups. (F) Quantitative measurement of chondrogenesis differentiation ability in (E) (n = 3, triplicates per group). All data are reported as mean ± SD. Statistical significance was determined by one-way ANOVA. ***p < 0.0001.

results showed that the phenotype of Ihh-deficient mice (Ihh^{cko}) closely mimicked that of humans with Ihh gene mutation-related skeletal dysplasia defects, including short stature with short spine and trunk, narrow thorax (Figures S1A–S1D), smaller skull, and shorter neck (Figure S1B) and extremity bones (Figures S1E and S1F).

SAG rescues defective chondrocyte proliferation and differentiation caused by Ihh ablation

To test whether defective chondrocyte function caused by loss of Ihh can be rescued by SAG treatment, we first performed *in vitro* analysis of chondrocytes isolated from Ihh-ablated mouse cartilage tissue and determined the ideal concentration used in the study (Figure S2). The results of bromodeoxyuridine (BrdU) staining showed that Ihh deletion inhibited chondrocyte proliferation, and this effect was rescued by SAG treatment (Figures 2A and 2B). To further investigate the effect of SAG on osteogenic and chondrogenic differentiation, Ihh-deficient chondrocytes were treated with or without SAG accompanied by either osteogenic medium for 21 days or chondrogenic medium for 14 days (Figure S3). The results showed that ablation of Ihh significantly inhibited the osteogenic and chondrogenic differentiation of Acan+ cells. Moreover, SAG treatment restored osteogenesis (Figures 2C and 2D) and chondrogenesis in Ihh-deficient chondrocytes (Figures 2E and 2F).

Ablation of Ihh does not affect cilia formation and orientation

The primary cilium plays a critical role in Hh signaling, and many features of ciliopathies are associated with abnormal Hh signaling.²² However, whether Hh also affects cilia formation remains unclear.

To answer this question, we isolated and cultured primary chondrocytes from cartilage tissue of Ihh^{fl/fl} control and Ihh^{cko} mice that were injected with TM at P3 and P5 and harvested at P30 *in vitro* or stained cilia in samples from different groups of mice *in vivo*. The isolated chondrocytes were treated with SAG for 24 h, and then ciliogenesis was analyzed by immunofluorescence staining of Arl13b (a primary cilia marker).²³ The results showed that cilia were present in all groups (Figure 3A). Quantitative analysis showed no significant differences in cilia number, length, or orientation among the wild-type, Ihh-deficient, and Ihh-deficient SAG treatment groups either *in vivo* or *in vitro* (Figure 3B; Figures S4A and S4B). These results indicated that Ihh is not essential for ciliogenesis and orientation.

SAG enhances Hh signaling activation by promoting Smo localization to cilia

Accumulation of the membrane protein Smo within the primary cilium is a key event in Hh signal activation.²² To test how ciliary Smo responds to SAG in Ihh-deficient cells, chondrocytes of articular cartilage isolated from TM-injected Acan-creERT;Ihh^{fl/fl} or Ihh^{fl/fl} mice were treated with SAG for 24 h, and then Smo and Gli1 localization was detected by immunofluorescence staining. Lower levels of Smo in the cilium or Gli1 protein in the nucleus were detected in Ihh-deficient chondrocytes than in control chondrocytes. In contrast, SAG treatment resulted in dramatically increased Smo translocation to the primary cilium and Gli1 accumulation in the nucleus (Figures 3C and 3D). These findings suggested that SAG enhances Hh signaling activation by promoting Smo localization to cilia.

SAG restores skeletal bone growth and increases the survival rate of Ihh-deficient mice

To evaluate the effect of SAG treatment on the survival rate, Ihh^{fl/fl} or Acan-creERT;Ihh^{fl/fl} mice were injected with TM at P3 and P5. Then,

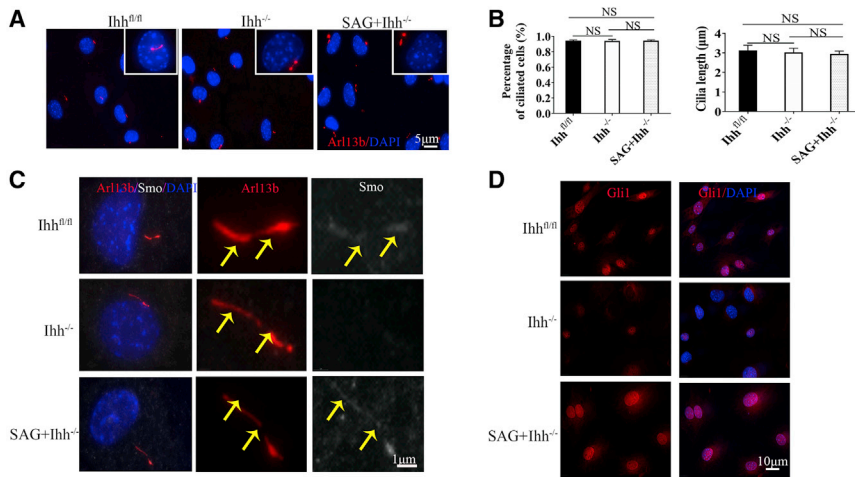


Figure 3. SAG promotes Hh activity by recruiting Smo in cilia

(A) Representative immunofluorescent staining images for Arl13b and DAPI showed the cilia length and percentage in chondrocytes from wild-type, *Ihh*-deficient, and *Ihh*-deficient with SAG treatment groups. Red: Arl13b; blue: DAPI. Bar is 5 μm (B) Quantitative measurements of primary cilia length and percentage of (A) ($n = 3$, triplicates per group with at least 100 cells analyzed in each group). (C) Immunofluorescent staining for Arl13b, Smo, and DAPI showing the smoothen expression and localization in chondrocyte from wild-type, *Ihh*-deficient, and *Ihh*-deficient with SAG treatment groups. Red: Arl13b; white: smoothen; blue: DAPI. Arrows depict the Smo localization in cilia. Bar is 1 μm (D) Immunofluorescent staining for Gli1 and DAPI showing the Gli1 expression and localization in chondrocyte from wild-type, *Ihh*-deficient, and *Ihh*-deficient with SAG treatment groups. Red: Gli1; blue: DAPI ($n = 3$, triplicates per group). Bar is 10 μm All data are reported as mean ± SD. Statistical significance was determined by one-way ANOVA. NS, not statistically significant.

the TM-injected male and female mice (mixed sexes in each group) were treated with vehicle ($n = 83$) or 20 μg/g SAG every other day starting from P7 ($n = 52$) or P14 ($n = 49$) up to P30.

At P7, the body weight and size of *Ihh*^{cko} mice were significantly lower than those of the control mice (Figures 4A–4D); however, the weight of SAG-treated *Ihh*^{cko} mice increased significantly at P30 (Figures 4E and 4G). Body length was also significantly increased in SAG-treated *Ihh*^{cko} mice compared with vehicle-treated *Ihh*^{cko} mice (Figures 4E–4G). The average body length was 133.2 ± 6.1 mm in the SAG-treated *Ihh*^{cko} group and 117.2 ± 6.9 mm in the vehicle-treated *Ihh*^{cko} group (Figures 4H and 4I). By inspecting all viscera (spleen, liver, heart, kidney, lung, and intestine) (Figure S5), we found no obvious abnormalities or tumorigenesis in the heart, lungs, kidneys, liver, or spleen, but intestinal hyperplasia was detected in 6.1% of SAG-treated mice in the *Ihh*^{cko} and *Ihh*^{fl/fl} groups.²⁰

We found that the survival rates of *Ihh*^{cko} mice treated with SAG at the earlier (P7) and later (P14) time points were 86.5% (45/52) and 83.6% (41/49), respectively, which were significantly higher than that of *Ihh*^{cko} mice treated with vehicle, which had a survival rate of 72.3% (60/83) (Figure 4J; Table 1); these results indicated that SAG treatment significantly improves the survival rate regardless of the time of administration. During the follow-up to P30, none of the animals in the vehicle-treated wild-type group died (0/83), while one animal died from bowel obstruction in the SAG-treated wild-type group (1/41). Notably, all vehicle-treated *Ihh*^{cko} mice (23/83) died due to respiratory failure caused by shortening of the ribs, which restricts pulmonary development.²⁰ In contrast, in the SAG-treated *Ihh*^{cko} mouse group, 7 of 101 mice died during the follow-up. Among these 7 mice, 5 mice died due to respiratory distress, and 2 mice died from bowel obstruction.^{19,20} These data indicated that SAG treatment significantly increases the survival rate of *Ihh*^{cko} animals.

SAG restores the growth of the appendicular skeleton in *Ihh*^{cko} mice

To further analyze the efficacy of SAG treatment, X-ray and micro-computed tomography (micro-CT) analyses were performed in SAG-treated *Ihh*^{cko} and control *Ihh*^{fl/fl} mice. The X-ray results showed a significant increase in the size of the limbs in SAG-treated *Ihh*^{cko} mice compared to that in vehicle-treated *Ihh*^{cko} littermates. The lengths of the femur and tibia bones in SAG-treated *Ihh*^{cko} mice were significantly increased by 67.4% and 33.1%, respectively, compared to those in the vehicle-treated *Ihh*^{cko} group (Figures 5A–5D). Similarly, the lengths of the humerus, radius, and ulna in SAG-treated *Ihh*^{cko} mice were significantly increased by 33.8%, 41.3%, and 66.4%, respectively, compared to those in vehicle-treated *Ihh*^{cko} mice (Figures S6A–S6D). Consistent with these results, micro-CT analysis showed marked restoration of bone mass and joint microarchitecture in SAG-treated *Ihh*^{cko} mice compared to vehicle-treated *Ihh*^{cko} mice (Figures 5E–5J). Trabecular bone parameters showed a tendency to improve in SAG-treated *Ihh*^{cko} mice, as the percentage of bone volume (BV/TV), trabecular number (Tb.N), and trabecular thickness (Tb.Th) were increased by 78%, 73.4%, and 90.3%, respectively, and the percentage of trabecular spacing (Tb.Sp) was decreased by 26% in SAG-treated *Ihh*^{cko} mice compared to vehicle-treated *Ihh*^{cko} mice (Figure 5H). Cortical bone parameters, including the percentage of cortical area (Ct.Ar), the total cross-sectional area (Tt.Ar), the cortical bone area fraction (Ct.Ar/Tt.Ar), and the cortical thickness (Ct.Th), were increased by 86%, 93.4%, 11.2%, and 54.8%, respectively, in SAG-treated *Ihh*^{cko} mice compared to vehicle-treated *Ihh*^{cko} mice (Figure 5J). These findings indicated that SAG treatment dramatically improved the osteopenia phenotype.

To determine whether SAG treatment affects anabolic bone formation, we measured bone formation parameters in both SAG- and vehicle-treated *Ihh*^{cko} mice by injecting fluorochrome into the mice at P21 and P27 and harvesting them at P30. As shown in Figure 5O,

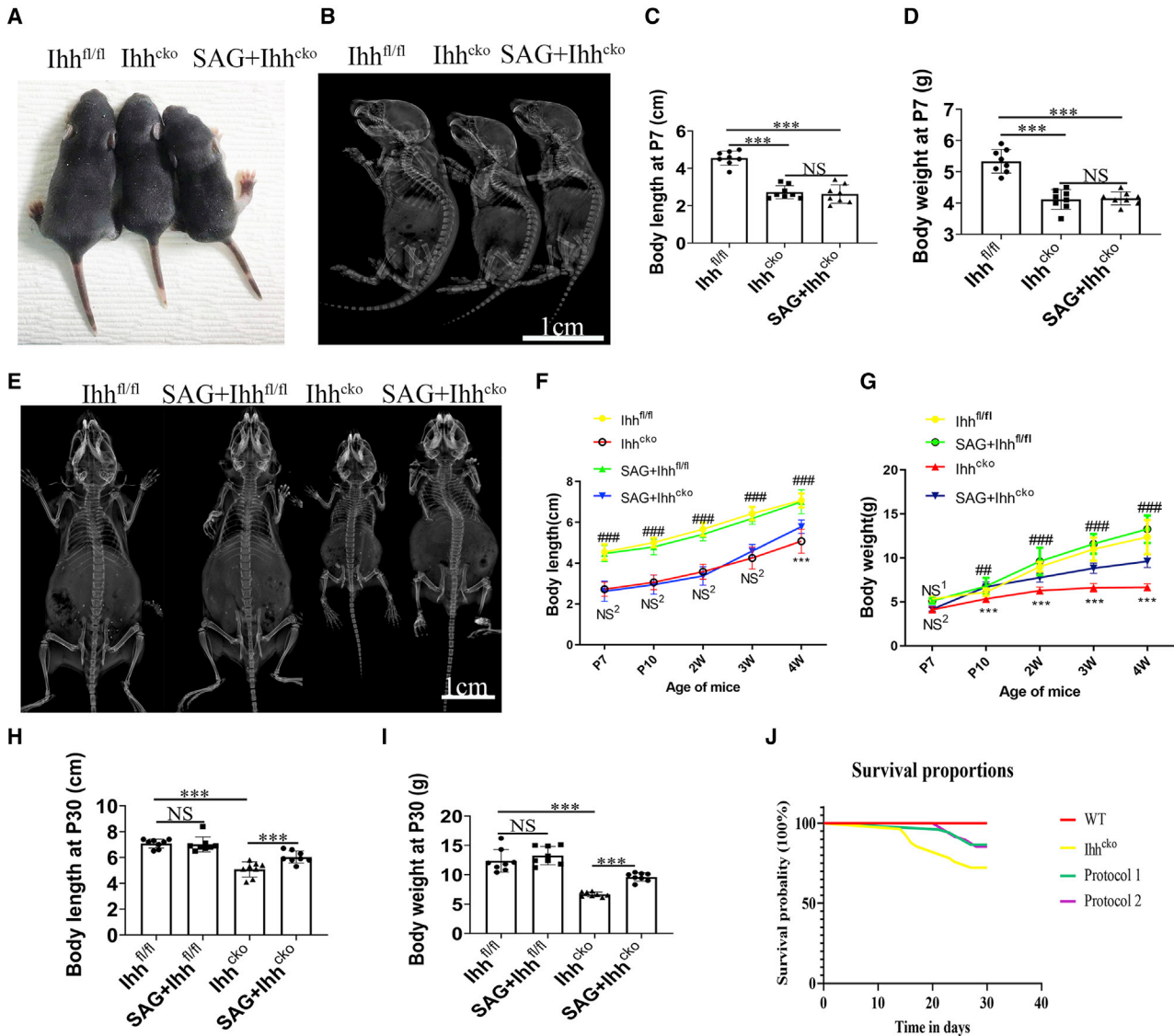


Figure 4. SAG restores skeletal defects in a mouse model of human *Ihh* gene mutation-related dysplasia

(A and B) Gross morphology and X-ray radiographs showed the mouse size and bone image in wild-type, vehicle-treated, and SAG-treated *Ihh^{cko}* mice at P7. Bar is 1cm (C and D) Quantitative analysis the body length and weight in (A) and (B) (n = 8 in each group). (E) X-ray radiographs illustrating the effect of SAG treatment on skeletal growth at P30. Wild-type and *Ihh*-deficient mice were subcutaneously injected with vehicle or SAG 20 μ g/g. Bar is 1cm (F and G) Quantitative analysis of the body length and weight from P7 to P30 (n = 8 in each group). NS1, SAG treated *Ihh^{cko}* compared with *Ihh^{cko}*, not statistically significant. NS2, *Ihh^{cko}* compared with *Ihh^{fl/fl}*, not statistically significant. ****Ihh^{cko}* compared with *Ihh^{fl/fl}*, p < 0.0001. ###SAG treated *Ihh^{cko}* compared with *Ihh^{cko}*, p < 0.0001. (H and I) Quantitative analysis of the body length and weight at P30 (n = 8 in each group). (G) The survival proportions analysis among each group. All data are reported as mean \pm SD. Statistical significance was determined by one-way ANOVA. ***p < 0.0001. NS, not statistically significant.

the bone formation rate per bone surface (BFR/BS) in the tibia was significantly inhibited in vehicle-treated *Ihh^{cko}* mice compared to *Ihh^{fl/fl}* control mice, but it was significantly rescued in SAG-treated *Ihh^{cko}* mice. Quantitative analysis showed that the MFR/BS was 0.18 mm³/mm²/day in vehicle-treated *Ihh^{cko}* mice and increased to 0.24 mm³/mm²/day in SAG-treated *Ihh^{cko}* mice (Figures 5K and 5L). These findings indicated that SAG promotes anabolic bone formation in *Ihh*-deficient mice.

SAG treatment rescues defective growth plate formation and the enchondroma-like phenotype caused by ablation of *Ihh*

By performing histological analyses of the bones of four limbs at P30, we found that Safranin O/fast green or alizarin red/Alcian blue staining showed cellular cartilage islands or rests in the metaphysis of several joint areas in all *Ihh^{cko}* mice, including the wrist joint (Figure 6A), the knee joint (Figure 6B), and the costochondral area (Figure 6C). In humans, enchondromas are defined by benign

Table 1. SAG treatment in *Ihh*^{CKO} mice

Treatment	Survival rate	Body length	Vertebral length	Femur length	Tibia length
WT (n = 83)	100%	–	–	–	–
<i>Ihh</i> ^{CKO} (n = 83)	72.3%	–	–	–	–
SAG (20 µg/g) (n = 52) protocol 1	86.5% ^a	+18.9% ^a	+32.1% ^a	+67.4% ^a	+33.1% ^a
SAG (20 µg/g) (n = 49) protocol 2	83.6% ^a	+15.5% ^a	+20.6% ^a	+20.4% ^a	+11.9% ^a

Survival rate and gain in length (percentage) for body, vertebral, femur, and tibia of SAG-treated mice compared with vehicle-treated mice. Protocol 1: 20 µg/g SAG every other day treating from P7 (n = 52) to P30. Protocol 2: 20 µg/g SAG every other day treating from P14 (n = 49) to P30.

^ap < 0.05 by one-way ANOVA test.

intramedullary neoplasms of hyaline cartilage. These ectopic cartilage rests most likely arise from foci of cartilage displaced or “remodeled out” of the growth plate.^{24–26} In our study, the cartilage islands were observed to connect the rests to the adjoining growth plate or cartilage, and the features of these tissues were highly similar to those of human enchondroma tissue^{25,27} (Figures 6A–6D). In addition, varying cellularity and disorganized cells were detected in a Safranin O-positive cartilage island, which closely mimics the histomorphology of human enchondromas^{28,29} (Figures 6B and 6C). BrdU staining showed that 73.2% of cells were BrdU+ in the enchondroma tissues of the *Ihh*^{CKO} group, but only 17.3% of cells were BrdU+ in the growth plates of *Ihh*^{fl/fl} mice, suggesting a significant increase in cell proliferation in enchondroma tissue (Figure S7). Given that *Ihh* deficiency results in enchondroma-like tissues but does not affect cilia formation (Figure S4), to further evaluate whether *Ihh* signaling and cilia formation are altered in human enchondroma, primary cilia were immunostained with an antibody against acetylated tubulin, and *Ihh* and *Gli1* were detected by immunofluorescence staining in human enchondroma samples and comparable articular cartilage samples. The results showed that both human enchondroma tissues and articular samples had similar cilia numbers and lengths (Figures S8A–S8C). The immunofluorescence staining results showed that the expression levels of *Ihh* and *Gli1* in enchondroma tissues were much lower than those in control tissues, suggesting that the reduction of *Ihh* expression is correlated with an enchondroma-like phenotype (Figures S8D and S8E). To further test whether SAG can inhibit enchondroma-like tissue formation, we treated *Ihh*^{CKO} mice with SAG. Treatment with SAG significantly reduced the formation of enchondroma-like tissue from 100% in vehicle-treated *Ihh*^{CKO} mice to only 16.7% in SAG-treated *Ihh*^{CKO} mice (17/101) (Figure 6D). Specifically, the results from alizarine red/Alcian blue and Safranin O/fast green staining of the ribs showed that deletion of *Ihh* caused enlarged chondro-osseous junctions of the ribs and numerous enchondroma-like tissues in the ribs and knee in *Ihh*^{CKO} mice, and these effects were significantly reduced by SAG treatment (Figures 6B and 6C). In addition, we also found that the percentage of enchondroma tissue with a diameter greater than 1 mm decreased from 76.6% in vehicle-treated *Ihh*^{CKO} mice to 8.9% in SAG-treated *Ihh*^{CKO} mice (Figure 6E). These results suggested that mutation of *Ihh* can cause enchondromas and that SAG can effectively reduce the incidence of enchondromas in *Ihh*-deficient mice. Moreover, Safranin O/fast green staining showed that SAG treatment significantly rescued growth plate and subchon-

dral bone formation in tibias of *Ihh*^{CKO} mice compared to vehicle treatment (Figure 6B). These results demonstrate that *Ihh* ablation in *Acan*+ cells caused enchondroma formation. SAG treatment promoted osteogenesis and chondrogenesis and reduced enchondroma formation in *Ihh*-deficient mice *in vivo*.

To characterize the effect of SAG on the expression of chondrocyte marker genes, mouse articular cartilage was isolated from *Ihh*^{fl/fl} and vehicle- and SAG-treated *Ihh*^{CKO} mice at P30, and then total RNA was extracted from these samples. Real-time RT-qPCR and western blot confirmed the loss of *Ihh* in the articular cartilage of the *Ihh*^{CKO} mice (Figure 6F; Figure S9). Moreover, we found that ablation of *Ihh* in cartilage significantly reduced the levels of *Ihh*, *Aggrecan*, *Sox9*, *Col2a1*, *patch1*, and *Gli1* to 0.1-, 0.2-, 0.2-, 0.3-, 0.2-, and 0.3-fold, respectively, in *Ihh*^{CKO} mouse cartilage compared with *Ihh*^{fl/fl} mouse cartilage (Figure 6F). In contrast, SAG treatment significantly upregulated the expression levels of these genes in *Ihh*^{CKO} mice compared with vehicle treatment (Figure 6F).

SAG restores the growth of the axial skeleton in *Ihh*-deficient mice

Patients with *Ihh* gene mutation-related syndromes often exhibit platyspondyly and spinal stenosis.³⁰ To test whether deletion of *Ihh* in *Acan*+ cells also affects spine and IVD development, we examined the spine and tail of *Ihh*^{CKO} mice and characterized the effects of SAG treatment. Coronal and sagittal X-ray analyses of the axial skeleton showed no obvious scoliosis or kyphosis in *Ihh*^{CKO} mice at P30 (Figures S1A–S1D). To assess the differences in the size of the axial skeleton, we measured the length of third lumbar vertebral bodies (L3), which are usually affected in *Ihh* gene mutation-related syndromes. MicroCT analysis showed that the length of L3 in *Ihh*^{CKO} mice was only 38.4% of the length in *Ihh*^{fl/fl} control mice. Treatment with SAG significantly increased the lumbar vertebral length of *Ihh*^{CKO} mice compared to the control treatment (+32.1%) (Figures 7A–7C). The tail length in SAG-treated mice was 60% longer than that in vehicle-treated *Ihh*^{CKO} mice at day 30 (Figures 7D and 7E). Analysis of Safranin O/fast green staining of the IVD in the L3–L4 of P30 mice further showed that the nucleus pulposus (NP) was surrounded by a well-formed annulus fibrosus (AF) in the *Ihh*^{fl/fl} IVD. However, ablation of *Ihh* led to IVD defects, including disrupted stereotypical columnar structure of the chondrocytes in the GP, reduced height of the endplate cartilage (EP) region, reduced number and size of

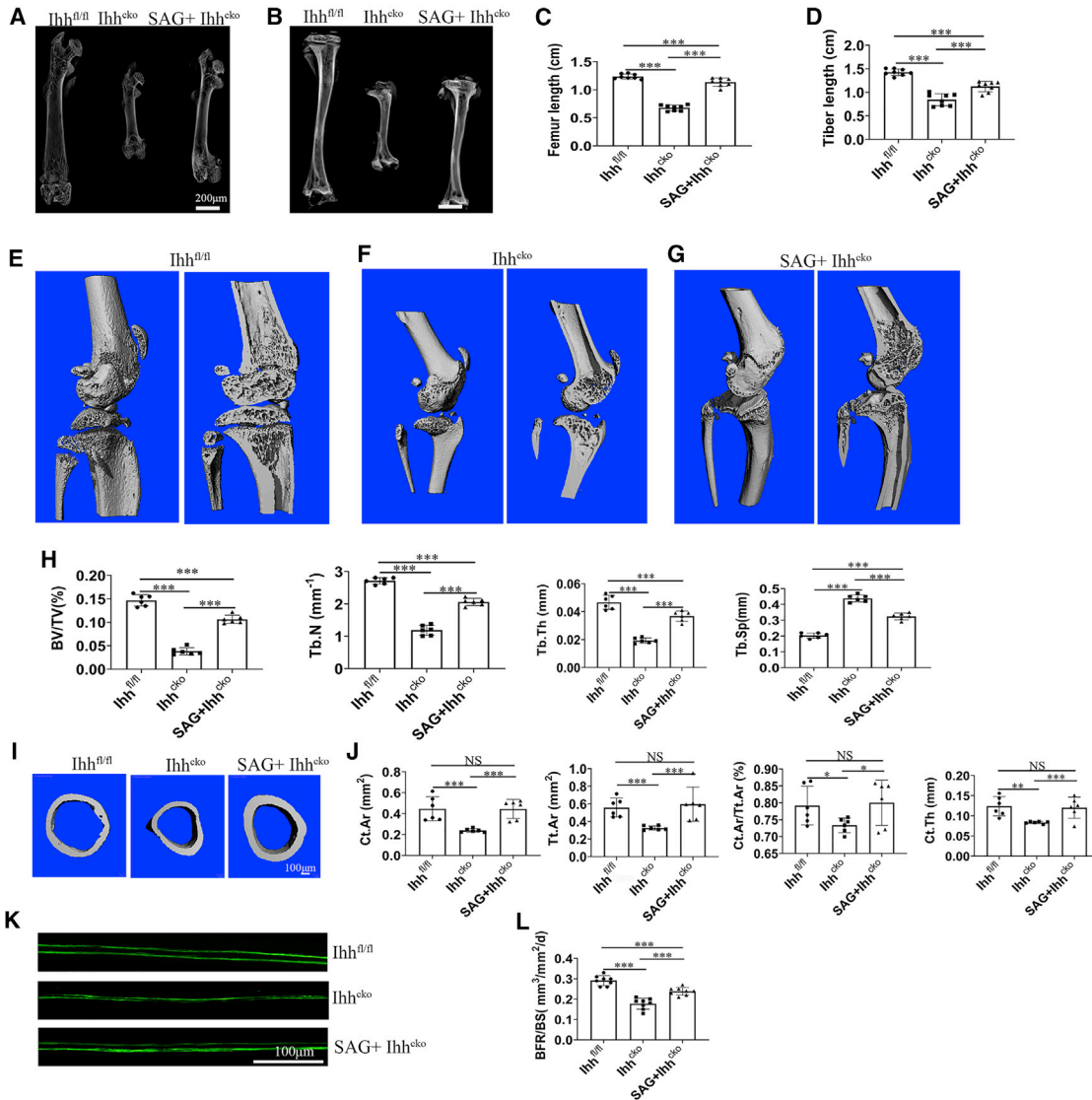


Figure 5. SAG increases the growth of the appendicular skeleton in *Ihh*-deficient mice

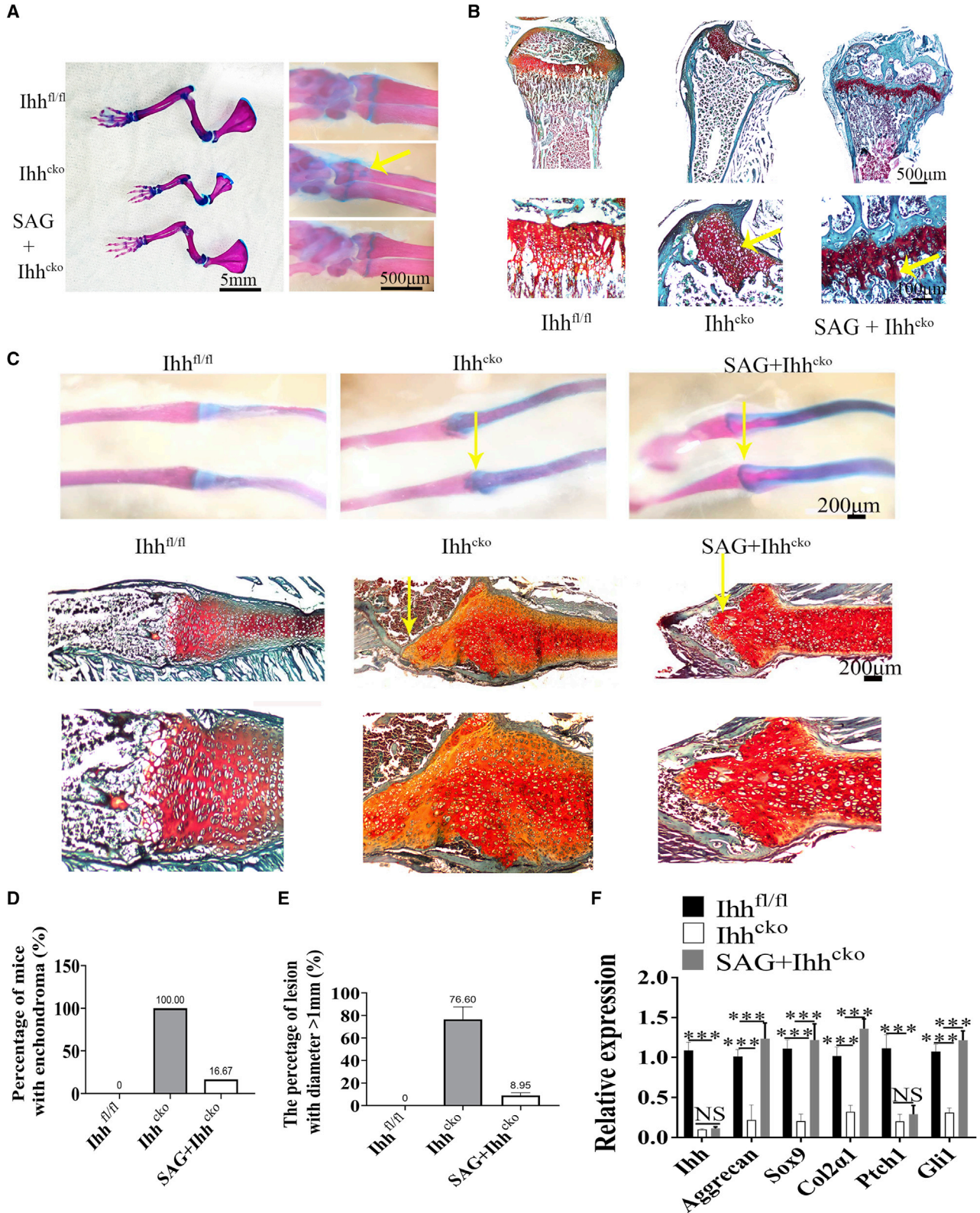
(A and B) Radiograph of femur and tibia in wild-type, vehicle-treated, and SAG-treated *Ihh*-deficient mice. Bar is 200 μ m. (C and D) Quantitative analysis of the femur and tibia length in (A) and (B) ($n = 8$). (E–G) Representative 3D micro-CT of the distal femur metaphysis cross-sectional area in wild-type, SAG-treated, and vehicle-treated *Ihh*-deficient mice. (H) Quantitative analysis of the bone volume (BV/TV), trabecular number (Tb.N), trabecular thickness (Tb.Th), and trabecular spacing (Tb.Sp) in femur trabecular bone ($n = 6$ in each group). (I) Representative 3D micro-CT of the distal femur metaphysis cortical bone ($n = 6$ in each group). Bar is 5 μ m. (J) Quantitative analysis of the cortical area (Ct.Ar), the total cross-sectional area (Tt.Ar), the cortical bone area fraction (Ct.Ar/Tt.Ar), and the cortical thickness (Ct.Th) ($n = 6$ in each group). (K) Dynamic histomorphometry of tibia after double calcein labeling. BFR/BS, bone formation rate per bone surface; BS, bone surface. Bar is 5 μ m. (L) Quantitative analysis of BFR/BS from double-calcein labeling. All data are reported as mean \pm SD. Statistical significance was determined by one-way ANOVA. * $p < 0.05$, ** $p < 0.01$, *** $p < 0.0001$. NS, not statistically significant.

EP cells, disrupted NP and AF patterns, and complete loss of gel-like matrix surrounding NP. SAG treatment evidently rescued GP, EP, AF, and NF formation and patterning in *Ihh*^{cko} mice (Figure 7F).

SAG restores skull and rib development impaired by *Ihh* deficiency

Given that *Ihh* gene mutation-related skeletal dysplasia display abnormalities in craniofacial development in human and mouse *Ihh*^{cko}

models, we therefore assessed whether early treatment with SAG could correct defective cartilage or bone development in the skull of *Ihh*^{cko} mice. The results from X-ray, micro-CT, and alizarine red/Alcian blue staining analyses revealed that SAG treatment increased the anterior-posterior length and width of the skull and reduced the brachycephalic appearance of *Ihh*^{cko} mice compared with vehicle treatment (Figures 8A–8D). Quantitative analysis showed that the skull width and skull length significantly increased by 2.4% and



(legend on next page)

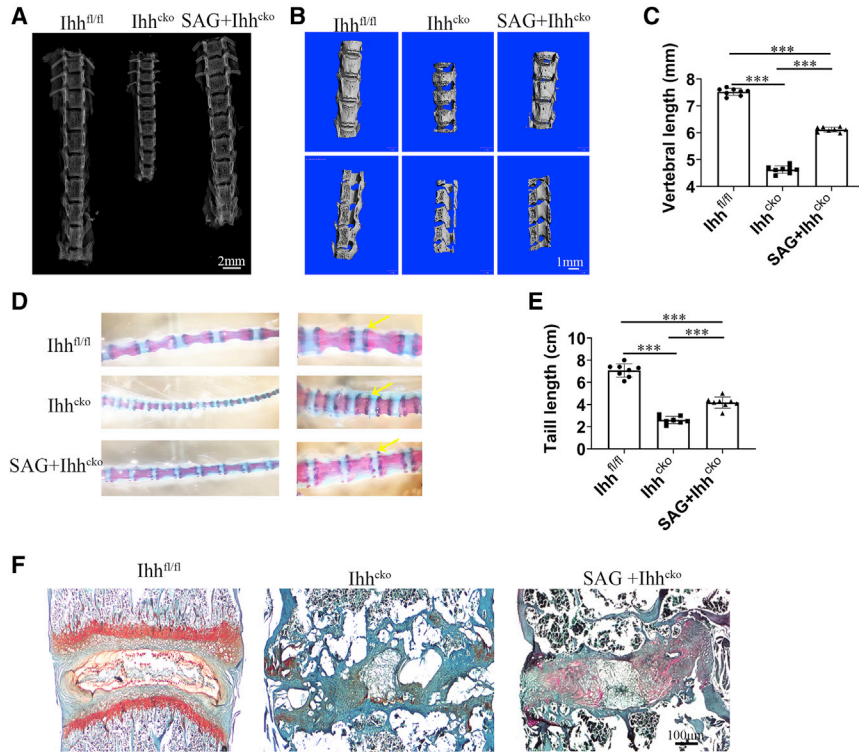


Figure 7. SAG rescues the growth of the axial skeleton detected in *Ihh*^{cko} mice

(A) Radiograph for spine of wild-type, vehicle-treated, and SAG-treated *Ihh*^{cko} mice. Bar is 2mm (B) Representative 3D microCT for the spine of wild-type, vehicle-treated, and SAG-treated *Ihh*^{cko} mice. Bar is 1mm. (C) Quantitative analysis of L3 vertebral length from wild-type, vehicle-treated, and SAG-treated *Ihh*^{cko} mice (n = 8 in each group). (D) Representative images of tail stained with Alcian blue (cartilage) and alizarin red (bone) in each group. (E) Quantitative analysis of tail length from wild-type, vehicle-treated, and SAG-treated *Ihh*^{cko} mice (n = 8 mice in each group). (F) Safranin O/fast green staining of coronal sections of L4-L5 IVD in wild-type, *Ihh* mutation, and SAG-treated *Ihh*^{cko} mice at P30. Bar is 100µm. All data are reported as mean ± SD. Statistical significance was determined by one-way ANOVA. ***p < 0.0001. NS, not statistically significant.

18.5%, respectively, in SAG-treated *Ihh*^{cko} mice compared to vehicle-treated *Ihh*^{cko} mice (Figure 8E). These results demonstrated that SAG treatment effectively corrects defective skull development.

Narrow thorax and smaller rib cage are often present in human *Ihh* gene mutation-related syndrome patients.^{1,3} Consistent with these observations, *Ihh*^{cko} mice also exhibited narrow thorax and smaller rib cage at P30. SAG treatment significantly corrected defective rib cage development and sternum length in *Ihh*^{cko} mice (Figure 8F). Specifically, the length of the sternum increased from 1.2 cm in vehicle-treated *Ihh*^{cko} mice to 1.56 cm in SAG-treated *Ihh*^{cko} mice (Figure 8G).

DISCUSSION

Various inactivation mutations of the gene encoding *Ihh* lead to loss of function of the *Ihh* ligand, resulting in skeletal chondrodysplasias, including acrocapitofemoral dysplasia, brachydactyly type A1, and human short stature.¹⁻³ Currently, there are no effective treatments for these diseases due to the lack of an ideal animal model.⁴ Since global deletion of *Ihh* at the embryonic stage or deletion of *Ihh* embryonically in type II collagen-positive (Col2+) cells causes mouse embry-

onic lethality,^{7,10,31} we generated TM-inducible *Ihh*^{cko} mice in this study by using *Acan*-creERT mice, which label the majority of *Acan*+ cells in the postnatal skeleton following TM injection at P3.^{18,21} At P30, we found that the phenotype of *Ihh*^{cko} mice closely mimics that of humans with *Ihh* gene mutation-related dysplasia.

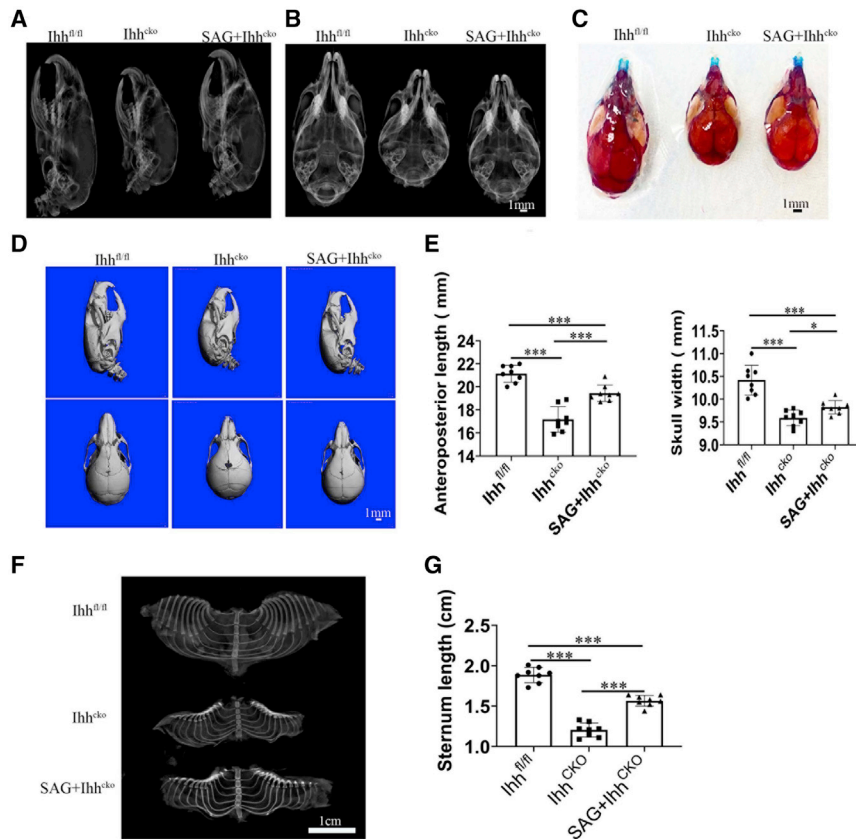
In vivo, we found for the first time that SAG treatment in *Ihh*^{cko} mice rescued growth plate and bone development, resulting in significant skeletal growth and a reduction in mortality, without evidence of toxicity. We also provide the first evidence that *Ihh* ablation in *Acan*+ cells led to the incidence of enchondromas and that this effect was significantly inhibited by SAG treatment.

The role of *Ihh* (or related signaling) in postnatal skeletal development has been investigated in several studies.^{8,32-35} Consistent with our results, postnatal deletion of *Ihh* with *Col2*-creERT by administration of TM caused premature fusion of growth plates of various endochondral bones in mice, resulting in dwarfism in mutant mice.

In the “canonical” Hh signaling cascade, binding of the Hh ligand to the *Ptch1* receptor leads to the release of the inhibition of the receptor *Smo*, thereby causing *Smo* trafficking into cilia to initiate a signaling cascade that culminates in the activation of *Gli* proteins (Figure S10). *Gli1* expression is one of the reliable indicators of downstream Hh pathway activity.^{16,17,36} SAG, a derivative of chlorobenzothiofene, is a Hh pathway agonist³⁷ that activates *Smo* to activate Hh¹⁹ in the presence of an intact primary cilium.³⁸⁻⁴⁴ Although Hynes et al.⁴⁵

Figure 6. SAG reduces the enchondroma incidence in *Ihh*-deficient mice

(A) Representative images of forelimbs stained with Alcian blue and alizarin red in wild-type, vehicle-treated, and SAG-treated *Ihh*^{cko} mice. (B) Representative images of tibia stained with Safranin O/fast green in wild-type, vehicle-treated, and SAG-treated *Ihh*^{cko} mice. (C) Representative images of ribs stained with Alcian blue and alizarin red and Safranin O/fast green from wild-type, vehicle-treated, and SAG-treated *Ihh*^{cko} mice at P30. Arrows depict the enchondroma-like tissues. Bar is 200µm (D) Quantitative analysis of enchondroma incidence in each group (n = 8/group). (E) Quantitative analysis of the percentage of lesion with diameter > 1 mm in each group (n = 8/group). (F) Real-time RT-qPCR analysis of *Ihh*, *Col2α1*, *Sox9*, *Aggrecan*, *Ptch1*, and *Gli1* expression levels in the cartilage tissue from each group (n = 3, triplicates per group). All data are reported as mean ± SD. Statistical significance was determined by one-way ANOVA. *p < 0.05, **p < 0.01, ***p < 0.0001. NS, not statistically significant.



demonstrated that SAG promotes ciliogenesis in renal epithelial cells with defective cilia formation, whether ablation of *Ihh* affects ciliogenesis is still unclear.^{39,46} Our study demonstrated that ablation of *Ihh* does not affect cilia formation and orientation but significantly disrupts cilia-mediated Hh signal transduction in the *Acan*⁺ cell lineage. Moreover, SAG treatment did not affect ciliogenesis. These results suggest that *Ihh* and SAG affect cilia-mediated Hh signaling activation but do not affect cilia assembly.

Although SAG administration has shown promising effects in preventing glucocorticoid-induced neonatal cerebellar injury²⁰ and treating Down syndrome,¹⁹ whether SAG is effective in the treatment of bone disorders is largely unknown.⁴² By performing immunofluorescence staining of *Smo*, we found that SAG enhanced Hh activity by promoting the ciliary localization of *Smo*. Both Aggrecan and collagen II are markers for chondrocyte differentiation. It was reported that SAG can promote chondrocyte differentiation.⁴⁷ In our study, SAG is a smooth agonist that functions to activate Hh signaling downstream of *Ihh*. Our study suggested that SAG can completely rescue the expression of downstream gene expression through regulating *Gli* activation, which drives downstream chondrocyte marker gene expression in *Ihh*-silenced chondrocytes *in vitro*. Consistent with these results, SAG treatment markedly suppressed growth plate defects, delayed differentiation and secondary ossification, and restored skull, vertebrae, and rib cage development in *Ihh*^{cko} mice. This evi-

dence suggests that SAG is a potential drug for correcting facial appearance and bone disorders and, most importantly, reducing the early mortality that often occurs in children with human *Ihh* gene mutation.¹⁻⁴

Human *Ihh* gene mutation-related skeletal dysplasias, such as acrocapitofemoral dysplasia, usually show anomalies including shorter spines, smaller vertebrae, short limbs, brachydactyly, and narrow thorax.¹ Similarly, *Ihh*^{cko} mice showed defective axial skeletons with smaller lumbar vertebral bodies, short limbs, narrow thorax, and impaired development of cartilage, IVDs, and lumbar vertebrae, suggesting that *Ihh*^{cko} mice are an ideal human *Ihh* gene mutation dysplasia-related mouse model. Moreover, our data demonstrated that SAG effectively treats the *Ihh* gene mutation-related dysplasia phenotype, and the efficacy of SAG treatment is dependent on the time of SAG administration. Treatment with SAG beginning on P14 efficiently increased the body weight and length of *Ihh*^{cko} mice compared to vehicle treatment. However, earlier treatment with SAG beginning on P7 was more effective in preventing the dwarfism phenotype compared to the treatment beginning on P14. These findings suggest that earlier administration of SAG to children will likely be more effective in correcting the defective skeletal and craniofacial development associated with skeletal dysplasia caused by *Ihh* gene mutation. Additionally, we noticed the improvement to the skull and rib are not as apparent as the femur/tibia. The exact reason remains unclear. It is known that *Ihh* regulates chondrocyte proliferation, differentiation, and osteoblast differentiation at the postnatal stage. It is possible that postnatal osteoblast differentiation and bone formation may count on the *Smo* signaling-dependent role of *Ihh*, while chondrocyte proliferation and differentiation rely on both the *Smo* signaling-dependent and *Smo* signaling-independent roles of *Ihh*. Thus, SAG can more effectively rescue the defective

bone but just partially rescue the growth plate and cartilage. Moreover, the expression pattern of Hh is varied in different bone tissues, and it is mainly located in prehypertrophic chondrocytes adjacent to the proliferation zone during development. The different rescue effects may also reflect the tissues sensitive extent or requirement to Ihh expression levels varied in different tissues.^{30,48} The specific mechanism needs to be investigated in the future. Noteworthy, although majority of cells in the growth plate are tdTomato positive, we found that some cells in the growth plate express lower or absent tdTomato fluorescence. Consistently, this phenomenon also occurs in the study by Ono et al.²¹ One possible reason is that Ihh was not completely ablated under tamoxifen induction, given that our real-time RT-PCR and western blot result showed that there are still low levels of Ihh expression in the bone tissues of Aggrecan-creERT;Ihh^{fl/fl} mice. Therefore, the Aggrecan-creERT;Ihh^{fl/fl} mouse model may not fully recapitulate the human phenotype with homozygous mutation of Ihh, but nonetheless it has a severe phenotype that can be rescued by SAG and is therefore still a valid model.

Although activation of the Hh pathway by SAG has been shown to be efficacious in correcting structural and cognitive deficits in a Down syndrome mouse model¹⁹ and preventing glucocorticoid-induced neonatal cerebellar injury,²⁰ there are some concerns about its clinical application due to the associated side effects, such as tumorigenesis.^{19,20} In this study, SAG-treated mice had no tumor formation or obvious complications during the 30-day follow-up. Consistent with this result, Das et al.¹⁹ found that SAG treatment did not cause medulloblastoma, precancerous lesions, or cancer in animals even at a dose of 140 µg/g per day.²⁰ Notably, in our study, a few animals treated with SAG had intestinal hyperplasia, showing increased thickness of the smooth muscle layer, which raises the possibility of bowel obstruction.²⁰ Thus, this study indicates that additional mechanistic and preclinical toxicity studies are needed to analyze the effect of SAG on intestinal tissue and function.

Some studies have indicated that Hh signaling is associated with various stages of carcinogenesis in different tumors.^{12,15,16,19,49} For example, in pancreatic and esophageal cancer, activation of the Hh signaling pathway was found in the early stages of tumors as well as in metastatic tumors.⁵⁰ Treatment of human chondrosarcoma SW1353 cells with Hh pathway inhibitor-4 (HPI-4) significantly decreased proliferation, invasion, and migration capacity.^{51,52} Another study demonstrated that knockdown of Gli1 expression by small interfering RNA (siRNA) downregulated the expression of the key Hh pathway components Ptch1 and Smo and reduced the growth and survival of chondrosarcoma cells.^{52,53} These studies provide a convincing rationale for investigating Hh pathway inhibitors as a novel therapeutic option for chondrosarcoma patients with aberrant activation of the Hh signaling pathway. Although preclinical data have demonstrated hyperactive Hh signaling in a wide range of malignancies, the clinical data from a phase II randomized placebo-controlled trial of Hh inhibitors in patients with advanced chondrosarcoma have been discouraging.¹⁴ Moreover, it was recently reported that Hh signaling is downregulated in several can-

cers and that its restoration suppresses tumor growth.¹⁵ In our study, we found for the first time that ablation of Ihh in Acan+ cells caused an enchondroma-like phenotype in the rib and growth plate regions and that activation of Hh signaling by SAG decreased the incidence and size of enchondroma-like tissue. Consistent with these findings, Rozeman et al.⁵⁴ also found that Hh signaling activity is reduced in some human enchondromas. However, the finding that chondrocyte-specific overexpression of Gli2, a downstream transcriptional activator of the Hh pathway, causes enchondroma⁴¹ suggests the possibility that a certain range of Hh levels is essential for normal physiological function, while overactivation or disruption of Hh signaling leads to enchondroma genesis, which needs to be further studied in the future.

MATERIALS AND METHODS

Mice

All procedures regarding housing, breeding, and the collection of animal tissues were performed according to protocols approved by the Institutional Animal Care and Use Committee (IACUC) of the University of Pennsylvania in accordance with the IACUC's relevant guidelines and regulations. All animals were of the C57BL strain.

TdTomato⁵⁵ and DTA^{fl/fl}⁵⁶ mice were purchased from Jackson Laboratory (Bar Harbor, ME, USA). Acan-creERT and Ihh^{fl/fl} mice were supplied by Eiki Koyama.¹⁸ Acan-creERT;Ihh^{fl/fl}, Acan-creERT;tdTomato, and Acan-creERT;DTA^{fl/fl} mice were generated by breeding Acan-creERT mice with Ihh^{fl/fl}, tdTomato, or DTA^{fl/fl} mice, respectively. TM (T5648, Sigma, St. Louis, MO, USA) solution preparation and administration were performed as previously described.⁵⁷ Briefly, TM was first dissolved in 100% ethanol (100 mg/mL) and then diluted with sterile corn oil to a final concentration of 10 mg/mL. For neonatal injection, Ihh^{fl/fl}, Acan-creERT;Ihh^{fl/fl}, Acan-creERT;tdTomato, and Acan-creERT;DTA^{fl/fl} mice were administered the same dose of TM (75 mg TM/kg body weight) at P3 and/or P5.

Preparation and systemic administration of SAG

SAG (B5837) was purchased from APExBIO Technology (Houston, TX, USA).¹⁹ The chlorobenzothiophene derivative SAG (molecular weight, 490.06) was dissolved in dimethyl sulfoxide (DMSO) to 5 mM and further diluted with normal saline or culture medium. Vehicle controls comprised saline containing an equivalent concentration of DMSO. P7 or P14 Acan-creERT;Ihh^{fl/fl} or Ihh^{fl/fl} pups were i.p. injected with SAG (20 µg/g) or vehicle every other day until they were harvested at P30. 10 nM SAG was used *in vitro*.⁵⁸

Human samples

Human samples were obtained from US Biomax (Rockville, MD, USA). Three enchondromas and three normal articular cartilage samples were analyzed for the presence of primary cilia.

H&E staining and histological measurements

Organs or human tissues were harvested and stored in 10% formalin for further histological analysis with standard paraffin-embedding

techniques. Using a standard microtome (RM2255, Leica), 6 μm sections were prepared and stained with H&E. Histological measurements were performed on randomly selected samples from all groups and were analyzed blindly by a pathologist. Organs were observed for macroscopic abnormalities such as modification of color or texture and presence of nodules. Microscopically, pathological criteria included but were not limited to modification of organ architecture or cell morphology; presence of fibrosis, cellular dysplasia, metaplasia, or atypia; and presence of inflammatory foci.

Alizarin red/Alcian blue staining

Alizarin red/Alcian blue staining was used to stain the mouse skeleton as described previously.^{57,59} Briefly, the samples were fixed with 90% ethanol and then stained with 0.01% Alcian blue solution (26385-01, Electron Microscopy Sciences, Hatfield, PA, USA) and 1% alizarin red S solution (A47503, Thomas Scientific, Swedesboro, NJ, USA). The stained skeleton samples were stored in glycerol.

Safranin O/fast green staining

Mouse IVDs, tibia, and ribs were excised, fixed with 10% natural buffered formalin, and decalcified in 10% ethylenediaminetetraacetic acid (EDTA) for 10 days at 4°C. The samples were embedded in paraffin. Using a standard microtome (RM2255, Leica), 6- μm sections were prepared and subsequently stained with Safranin O/fast green stain to visualize cartilage and assess proteoglycan content as described previously.^{38,57} The slides were stained with Weigert's iron hematoxylin and fast green and then stained with 0.1% Safranin O solution.

Cell isolation and culture

Primary chondrocytes were isolated using published methods.^{60,61} Briefly, TM-injected $\text{Ihh}^{\text{fl/fl}}$ and $\text{Acan-creERT};\text{Ihh}^{\text{fl/fl}}$ mice were euthanized at P10. Articular cartilage from the femoral heads, femoral condyles, and tibia plateaus was isolated, followed by incubation with collagenase type IV (Worthington, Lakewood, NJ, USA) (3 mg/mL) for 45 min at 37°C. Cartilage pieces were obtained and incubated in 0.5 mg/mL collagenase type IV solution overnight at 37°C. The cells were then filtered through a 40- μm cell strainer and cultured in DMEM culture medium containing 10% FBS.

In vitro cell differentiation assay

Chondrocytes isolated from Ihh^{cko} mice were treated with 10 nM SAG. The three groups of chondrogenic and osteoblastic differentiation were induced with different differentiation media and detected by staining with Alcian blue (26385-01, Electron Microscopy Sciences) and alizarin red S (A47503, Thomas Scientific, Swedesboro, NJ, USA), respectively. For osteogenesis, the cells were induced with osteogenic media for 21 days as described previously.⁶² For chondrogenesis, micromass culture was performed as described previously.⁶⁰ Briefly, micromasses were obtained by pipetting 20 μL of primary chondrocytes into individual wells of 24-well plates. Following a 3-h attachment period without medium, the growth medium was gently added into the wells with cells. Differentiation was induced by insulin transferrin selenium (ITS) supplementation for

14 days. Quantitative analysis of Alcian blue and alizarin red S was performed as described previously.⁶⁰

Immunofluorescence staining

Mice or human tissues were harvested and stored in 10% formalin for further histological analysis with standard paraffin-embedding techniques. Using a standard microtome (RM2255, Leica), 6- μm sections were prepared. The sections were deparaffinized and incubated either in microwaved citrate buffer for 20 min or with proteinase K (20 $\mu\text{g}/\text{mL}$, D3001-2-5, Zymo Research, Irvine, CA, USA) for 10 min at room temperature. Subsequently, the sections were blocked in 5% normal serum (10,000 C, Thermo Fisher Scientific, Waltham, MA, USA) in PBS-T (0.4% Triton X-100 in PBS). Then, the sections were incubated with antibodies against Ihh (1:100, ab34710, Abcam, Waltham, MA, USA), Gli1 (1:100, ab34712, Abcam, Waltham, MA, USA), Smo (1:100, ab34710, Abcam, Waltham, MA, USA), acetylated tubulin (1:500, T6793, Sigma, St. Louis, MO, USA), or Arl13b (1:100, ab34710, Abcam, Waltham, MA, USA) in blocking buffer at 4°C overnight. Then, the sections were washed 3 times with PBS and incubated with Alexa Fluor 488-conjugated anti-rabbit (1:200, A11008, Invitrogen) or Alexa Fluor 647-conjugated anti-mouse (1:200, A-21236, Invitrogen) secondary antibody for 1 h. Coverslips were mounted with FluoroShield (F6057, Sigma-Aldrich, St. Louis, MO, USA).

Chondrocytes harvested from Ihh^{cko} mice were treated with SAG for 24 h and then serum-starved for 48 h, washed with PBS, and fixed with 4% paraformaldehyde at room temperature. The fixed cells from the control and SAG-treated groups were permeabilized with 0.05% Triton X-100 and then incubated with antibodies against Ihh (1:100, ab34710, Abcam, Waltham, MA, USA), Gli1 (1:100, ab34712, Abcam, Waltham, MA, USA), Smo (1:100, ab34710, Abcam, Waltham, MA, USA), or Arl13b (1:100, ab34710, Abcam, Waltham, MA, USA) in blocking buffer at 4°C overnight. Then, the samples were washed 3 times with PBS and incubated with Alexa Fluor 488-conjugated anti-rabbit (1:200, A11008, Invitrogen, Waltham, MA, USA) or Alexa Fluor 647-conjugated anti-mouse (1:200, A-21236, Invitrogen, Waltham, MA, USA) secondary antibody for 1 h. Coverslips were mounted with FluoroShield (F6057, Sigma-Aldrich, St. Louis, MO, USA).

To quantify cilia length, z stack images of multiple fields were randomly captured. The cilia were measured by drawing a boundary across the length of the primary cilium using the freehand tool and measuring cilia length by using ImageJ software. A total of at least 200 cells from each section of each sample (40 \times magnification, five sections collected per sample) were measured. To quantify ciliated cell percentage, z stack images of multiple fields were randomly collected. Ciliated cells were counted on each image. At least 30 images were measured. The percentage of ciliated cells was calculated from the ratio of the number of ciliated cells to the total number of cells observed in each compartment and each sample (40 \times magnification, five sections collected per sample). Six mice were evaluated in each group. The average ciliated cell percentage and cilia length in each sample were pooled and calculated by two authors.³⁸

Table 2. Primers

	Forward	Reverse
Ihh	5'-TTCGGCCGCTGCCAAGACAG-3'	5'-GCCACGTGGGTGGAGACAGC-3'
Sox9	5'-TCCCCGCAACAGATCTCTA-3'	5'-AGGTGGAGTAGAGCCCTGAG-3'
Aggrecan	5'-CGTTGCAGACCAGGAGCAAT-3'	5'-AGGAGTGACAATGCTGCTCA-3'
Patch	5'-GACCGCCTTGC CTCAACCC-3'	5'-CAGGGCGTGAGCGCTGACAA-3'
Gli1	5'-GAG TGCCATGCCGAGCAGAGA-3'	5'-ACTGGCCCTCCGAGTGACCC-3'
Col2 α 1	5'-GCAGAATGGGCAGAGGTATAA-3'	5'-AGTCTGGGTCTTACAGATAATG-3'
ALP	5'-AGTCAGGTTGTTCCGATTCA-3'	5'-GGGCATTGTGACTACCACCTC-3'
Runx2	5'-AAATTGCAGGCTTCGTGGTTGAGG-3'	5'-AATGGCTGTATGGTGAGGCTGGTA-3'
Osterix	5'-AATCCTATTGCGGTTTCC-3'	5'-TCTACGAGCAAGGTCTCCAC-3'
Osteocalcin	5'-GCGCTCTGTCTCTGACCT-3'	5'-ACCACTCCAGCACAACTCT-3'
Col1 α 1	5'-GAGGGAGTTTACACGAAGCA-3'	5'-AAAGAAGCAGCTCTGGTTTG-3'
GAPDH	5'-TGTGTCCGTCGTGGATCTGA-3'	5'-TTGCTGTTGAAGTCGCAGGAG-3'

BrdU cell proliferation assay

Cells isolated from *Ihh*^{cko} mice were treated with 10 nM SAG for 24 h. The cultures were incubated with BrdU solution (1:100, 000103, Invitrogen, Waltham, MA, USA) for 20 h and stained with BrdU with a BrdU staining kit (1:100, MA3071, Invitrogen, Waltham, MA, USA) according to the manufacturer's instructions. Sections (6 μ m thick) were prepared as described for immunofluorescence staining and stained with a BrdU staining kit (1:100, MA3071, Invitrogen, Waltham, MA, USA) according to the manufacturer's instructions. The BrdU-positive cell number and total cell number were counted in 10 images per sample. The number of BrdU-positive cells is indicated as a percentage of the total cell number. The BrdU assay was repeated using three independent samples for each experimental group.

X-ray and micro-CT scan

X-rays of all skeletons were taken with a Faxitron X-ray machine (Edimex). The total length was measured from the nose to the end of the last caudal vertebra; the tail was measured starting at the first caudal vertebra examined with X-ray.

Quantitative analysis of the gross bone morphology and micro-architecture was performed with a micro-CT system and software (Micro-CT 35, Scanco Medical AG, Brüttisellen, Switzerland) in the Penn Center for Musculoskeletal Disorders (PCMD) at the University of Pennsylvania.⁶³ Briefly, the lumbar spine (L3–L5), lower limbs, or skull of *Ihh*^{fl/fl}, vehicle-treated, and SAG-treated *Ihh*^{cko} mice at P30 were fixed, scanned, and reconstituted into three-dimensional images. The cross-sectional scans were analyzed to evaluate the changes in the entire femur. The regions of interest (ROIs) were then compiled into three-dimensional (3D) datasets using a Gaussian filter (sigma = 1.2, support = 2) to reduce noise and converted to binary images with a fixed grayscale threshold of 316. Two hundred slices (2 mm) above the highest point of the growth plate were contoured for trabecular bone analysis, including the percentage of bone volume (BV/TV, %), trabecular number (Tb.N, mm⁻¹), trabecular thickness (Tb.Th,

mm), and trabecular spacing (Tb.Sp, mm). The cortical bone architecture was assessed at the distal femoral metaphysis and midshaft. Fifty slices (0.5 mm) of the femur midshaft were contoured for cortical bone analysis, including the cortical area (Ct.Ar, mm²), total area (Tt.Ar, mm²), cortical area fraction (Ct.Ar/Tt.Ar, %), and cortical thickness (Ct.Th, mm). Six mice were evaluated in each group.

Real-time RT-PCR analysis

Articular cartilage tissues were dissected from the knees of *Ihh*^{fl/fl} and vehicle- and SAG-treated *Ihh*^{cko} mice at P30 and immediately placed in TRIzol for total RNA isolation (15596018, Thermo Fisher Scientific) according to the manufacturer's instructions. cDNA was synthesized from 2 μ g of total RNA. qPCR was performed with SYBR Green PCR Master Mix (B21202, Bimake). All qPCRs were run in triplicate, and gene expression was normalized to the expression of GAPDH. The calculation of relative expression was performed according to the 2^{-ddCT} method. Each reaction was run in triplicate and independently repeated three times. The sequences and product lengths for each primer pair are included in Table 2.

Western blotting

Western blotting was performed to detect *Ihh* expression using the rabbit anti-*Ihh* antibody (1:400, sc-271101, Santa Cruz) as described previously.⁵⁹ Long bone tissues from 4-week-old *Ihh*^{fl/fl} and *Ihh*^{cko} mice were lysed with NP 40 buffer (1% NP-40, 0.15 M NaCl, 50 mM Tris [pH 8.0]) containing a protease inhibitor cocktail (PI78441, Fisher Scientific). The cell lysates were centrifuged at 12,000 \times g for 10 min at 4°C, and the supernatants were stored at -80°C. Protein concentration was measured using BCA protein assay reagent (23225, Fisher Scientific). Equal amounts of protein (approximately 20 mg) were denatured in SDS containing Laemmli buffer and separated in 10% SDS-PAGE gels. Proteins were transferred to polyvinylidene difluoride membranes (Millipore) in buffer containing 25 mM Tris, 192 mM glycine, and 20% methanol. The membranes were blocked with 5% non-fat milk, incubated with a primary antibody overnight at 4°C, and then incubated with the horseradish

peroxidase (HRP)-conjugated goat anti-rabbit IgG antibody (1:10,000, A-11034, Novex) at room temperature for 1 h. Enhanced chemiluminescence was performed with Western Bright enhanced chemiluminescence E(CL)HRP (Biorad). β -actin (1:2,000, sc-47778, Santa Cruz) was probed as the internal control.

Statistics

All data are presented as the mean \pm SD. Bartlett's test of variance was performed to determine the appropriate statistical tests. Student's t test was performed for comparisons between two groups, and one-way ANOVA followed by Tukey's multiple comparison test was performed for grouped samples. The numbers of animals and experimental repetitions are presented in the figure legends. The program GraphPad Prism (GraphPad Software, San Diego, CA, USA) was used for these analyses and survival rate analysis. $p < 0.05$ was considered to be significant. NS denotes not significant.

SUPPLEMENTAL INFORMATION

Supplemental information can be found online at <https://doi.org/10.1016/j.omtm.2021.09.015>.

ACKNOWLEDGMENTS

Research reported in this publication was supported by the National Institute of Dental and Craniofacial Research, the National Institute of Arthritis and Musculoskeletal and Skin Diseases, and National Institute on Aging, part of the National Institutes of Health, under award numbers DE023105, AR066101, and AG048388 to Dr. Shuying Yang. The research sponsored by the Shanghai Sailing Program (21YF1436400) and National Natural Science Foundation of China (82102608) to X.L. X.L. was supported by China Scholarship Council (CSC) grant 201706260178. The content is solely the responsibility of the authors and does not necessarily represent the official views of the National Institutes of Health. The authors acknowledge Penn Center for Musculoskeletal Disorders for providing access to the microCT instrument and software (NIH/NIAMS P30 AR069619).

AUTHOR CONTRIBUTIONS

X.L. conceived the idea and performed the experiments, interpreted the data, and wrote the initial draft of the manuscript. Shuting Yang and Z.C. managed mice colonies and assisted with the experiments. S.Y. supervised the study and revised the manuscript. E.K. provided critical suggestions and reagents during the study.

DECLARATION OF INTERESTS

The authors declare no competing interests.

REFERENCES

- Hellemans, J., Coucke, P.J., Giedion, A., De Paepe, A., Kramer, P., Beemer, F., and Mortier, G.R. (2003). Homozygous mutations in IHH cause acrocapitofemoral dysplasia, an autosomal recessive disorder with cone-shaped epiphyses in hands and hips. *Am. J. Hum. Genet.* *72*, 1040–1046.
- Liu, M., Wang, X., Cai, Z., Tang, Z., Cao, K., Liang, B., Ren, X., Liu, J.Y., and Wang, Q.K. (2006). A novel heterozygous mutation in the Indian hedgehog gene (IHH) is associated with brachydactyly type A1 in a Chinese family. *J. Hum. Genet.* *51*, 727–731.
- Ma, G., Yu, J., Xiao, Y., Chan, D., Gao, B., Hu, J., He, Y., Guo, S., Zhou, J., Zhang, L., et al. (2011). Indian hedgehog mutations causing brachydactyly type A1 impair Hedgehog signal transduction at multiple levels. *Cell Res.* *21*, 1343–1357.
- Vasques, G.A., Funari, M.F.A., Ferreira, F.M., Aza-Carmona, M., Senthordi-Montané, L., Barraza-García, J., Lerario, A.M., Yamamoto, G.L., Naslavsky, M.S., Duarte, Y.A.O., et al. (2018). IHH Gene Mutations Causing Short Stature With Nonspecific Skeletal Abnormalities and Response to Growth Hormone Therapy. *J. Clin. Endocrinol. Metab.* *103*, 604–614.
- Senthordi-Montané, L., Benito-Sanz, S., Aza-Carmona, M., Pereda, A., Parrón-Pajares, M., de la Torre, C., Vasques, G.A., Funari, M.F.A., Travessa, A.M., Dias, P., et al. (2020). Clinical and Molecular Description of 16 Families With Heterozygous IHH Variants. *J. Clin. Endocrinol. Metab.* *105*, dgaa218.
- Maeda, Y., Schipani, E., Densmore, M.J., and Lanske, B. (2010). Partial rescue of postnatal growth plate abnormalities in *Ihh* mutants by expression of a constitutively active PTH/PTHrP receptor. *Bone* *46*, 472–478.
- St-Jacques, B., Hammerschmidt, M., and McMahon, A.P. (1999). Indian hedgehog signaling regulates proliferation and differentiation of chondrocytes and is essential for bone formation. *Genes Dev.* *13*, 2072–2086.
- Maeda, Y., Nakamura, E., Nguyen, M.T., Suva, L.J., Swain, F.L., Razzaque, M.S., Mackem, S., and Lanske, B. (2007). Indian Hedgehog produced by postnatal chondrocytes is essential for maintaining a growth plate and trabecular bone. *Proc. Natl. Acad. Sci. USA* *104*, 6382–6387.
- Gao, B., Hu, J., Stricker, S., Cheung, M., Ma, G., Law, K.F., Witte, F., Briscoe, J., Mundlos, S., He, L., et al. (2009). A mutation in *Ihh* that causes digit abnormalities alters its signalling capacity and range. *Nature* *458*, 1196–1200.
- Long, F., Zhang, X.M., Karp, S., Yang, Y., and McMahon, A.P. (2001). Genetic manipulation of hedgehog signaling in the endochondral skeleton reveals a direct role in the regulation of chondrocyte proliferation. *Development* *128*, 5099–5108.
- Raleigh, D.R., and Reiter, J.F. (2019). Misactivation of Hedgehog signaling causes inherited and sporadic cancers. *J. Clin. Invest.* *129*, 465–475.
- Epstein, E.H. (2008). Basal cell carcinomas: attack of the hedgehog. *Nat. Rev. Cancer* *8*, 743–754.
- Polychronidou, G., Karavasilis, V., Pollack, S.M., Huang, P.H., Lee, A., and Jones, R.L. (2017). Novel therapeutic approaches in chondrosarcoma. *Future Oncol.* *13*, 637–648.
- Italiano, A., Le Cesne, A., Bellera, C., Piperno-Neumann, S., Duffaud, F., Penel, N., Cassier, P., Domont, J., Takebe, N., Kind, M., et al. (2013). GDC-0449 in patients with advanced chondrosarcomas: a French Sarcoma Group/US and French National Cancer Institute Single-Arm Phase II Collaborative Study. *Ann. Oncol.* *24*, 2922–2926.
- Gerling, M., Büller, N.V., Kirn, L.M., Joost, S., Frings, O., Englert, B., Bergström, Å., Kuiper, R.V., Blaas, L., Wielenga, M.C., et al. (2016). Stromal Hedgehog signalling is downregulated in colon cancer and its restoration restrains tumour growth. *Nat. Commun.* *7*, 12321.
- Bale, A.E. (2002). Hedgehog signaling and human disease. *Annu. Rev. Genomics Hum. Genet.* *3*, 47–65.
- Yuan, X., and Yang, S. (2015). Cilia/Ift protein and motor-related bone diseases and mouse models. *Front. Biosci.* *20*, 515–555.
- Kurio, N., Saunders, C., Bechtold, T.E., Salhab, I., Nah, H.D., Sinha, S., Billings, P.C., Pacifici, M., and Koyama, E. (2018). Roles of *Ihh* signaling in chondrogenitor function in postnatal condylar cartilage. *Matrix Biol.* *67*, 15–31.
- Das, I., Park, J.M., Shin, J.H., Jeon, S.K., Lorenzi, H., Linden, D.J., Worley, P.F., and Reeves, R.H. (2013). Hedgehog agonist therapy corrects structural and cognitive deficits in a Down syndrome mouse model. *Sci. Transl. Med.* *5*, 201ra120.
- Heine, V.M., Griveau, A., Chapin, C., Ballard, P.L., Chen, J.K., and Rowitch, D.H. (2011). A small-molecule smoothened agonist prevents glucocorticoid-induced neonatal cerebellar injury. *Sci. Transl. Med.* *3*, 105ra104.
- Ono, N., Ono, W., Nagasawa, T., and Kronenberg, H.M. (2014). A subset of chondrogenic cells provides early mesenchymal progenitors in growing bones. *Nat. Cell Biol.* *16*, 1157–1167.
- Bangs, F., and Anderson, K.V. (2017). Primary Cilia and Mammalian Hedgehog Signaling. *Cold Spring Harb. Perspect. Biol.* *9*, a028175.
- Li, X., Yang, S., Deepak, V., Chinipardaz, Z., and Yang, S. (2021). Identification of Cilia in Different Mouse Tissues. *Cells* *10*, 1623.

24. Walden, M.J., Murphey, M.D., and Vidal, J.A. (2008). Incidental enchondromas of the knee. *AJR Am. J. Roentgenol.* *190*, 1611–1615.
25. McFarlane, J., Knight, T., Sinha, A., Cole, T., Kiely, N., and Freeman, R. (2016). Exostoses, enchondromatosis and metachondromatosis; diagnosis and management. *Acta Orthop. Belg.* *82*, 102–105.
26. Cantley, L., Saunders, C., Guttenberg, M., Candela, M.E., Ohta, Y., Yasuhara, R., Kondo, N., Sgariglia, F., Asai, S., Zhang, X., et al. (2013). Loss of β -catenin induces multifocal periosteal chondroma-like masses in mice. *Am. J. Pathol.* *182*, 917–927.
27. Hopyan, S., Gokgoz, N., Poon, R., Gensure, R.C., Yu, C., Cole, W.G., Bell, R.S., Jüppner, H., Andrulis, I.L., Wunder, J.S., and Alman, B.A. (2002). A mutant PTH/PTHrP type I receptor in enchondromatosis. *Nat. Genet.* *30*, 306–310.
28. Weiner, S.D. (2004). Enchondroma and chondrosarcoma of bone: clinical, radiologic, and histologic differentiation. *Instr. Course Lect.* *53*, 645–649.
29. Shariat Torbaghan, S., Ashouri, M., Jalayer Naderi, N., and Baherini, N. (2011). Histopathologic Differentiation between Enchondroma and Well-differentiated Chondrosarcoma: Evaluating the Efficacy of Diagnostic Histologic Structures. *J. Dent. Res. Dent. Clin. Dent. Prospect.* *5*, 98–101.
30. Yang, J., Andre, P., Ye, L., and Yang, Y.Z. (2015). The Hedgehog signalling pathway in bone formation. *Int. J. Oral Sci.* *7*, 73–79.
31. Long, F., Joeng, K.S., Xuan, S., Efstratiadis, A., and McMahon, A.P. (2006). Independent regulation of skeletal growth by Ihh and IGF signaling. *Dev. Biol.* *298*, 327–333.
32. Wu, Q., Chen, D., Zuscik, M.J., O’Keefe, R.J., and Rosier, R.N. (2008). Overexpression of Smurf2 stimulates endochondral ossification through upregulation of beta-catenin. *J. Bone Miner. Res.* *23*, 552–563.
33. Long, F., Chung, U.I., Ohba, S., McMahon, J., Kronenberg, H.M., and McMahon, A.P. (2004). Ihh signaling is directly required for the osteoblast lineage in the endochondral skeleton. *Development* *131*, 1309–1318.
34. Long, F., and Ornitz, D.M. (2013). Development of the endochondral skeleton. *Cold Spring Harb. Perspect. Biol.* *5*, a008334.
35. Enomoto-Iwamoto, M., Nakamura, T., Aikawa, T., Higuchi, Y., Yuasa, T., Yamaguchi, A., Nohno, T., Noji, S., Matsuya, T., Kurisu, K., et al. (2000). Hedgehog proteins stimulate chondrogenic cell differentiation and cartilage formation. *J. Bone Miner. Res.* *15*, 1659–1668.
36. Shi, Y., He, G., Lee, W.C., McKenzie, J.A., Silva, M.J., and Long, F. (2017). Gli1 identifies osteogenic progenitors for bone formation and fracture repair. *Nat. Commun.* *8*, 2043.
37. Frank-Kamenetsky, M., Zhang, X.M., Bottega, S., Guicherit, O., Wichterle, H., Dudek, H., Bumcrot, D., Wang, F.Y., Jones, S., Shulok, J., et al. (2002). Small-molecule modulators of Hedgehog signaling: identification and characterization of Smoothened agonists and antagonists. *J. Biol. Chem.* *277*, 1040–1048.
38. Bosakova, M., Abraham, S.P., Nita, A., Hrubá, E., Buchtová, M., Taylor, S.P., Duran, I., Martin, J., Svozilová, K., Barta, T., et al.; University of Washington Center for Mendelian Genomics (2020). Mutations in GRK2 cause Jeune syndrome by impairing Hedgehog and canonical Wnt signaling. *EMBO Mol. Med.* *12*, e11739.
39. de Andrea, C.E., Wiweger, M., Prins, F., Bovée, J.V., Romeo, S., and Hogendoorn, P.C. (2010). Primary cilia organization reflects polarity in the growth plate and implies loss of polarity and mosaicism in osteochondroma. *Lab. Invest.* *90*, 1091–1101.
40. Liu, H., Kiseleva, A.A., and Golemis, E.A. (2018). Ciliary signalling in cancer. *Nat. Rev. Cancer* *18*, 511–524.
41. Ho, L., Ali, S.A., Al-Jazrawe, M., Kandel, R., Wunder, J.S., and Alman, B.A. (2013). Primary cilia attenuate hedgehog signalling in neoplastic chondrocytes. *Oncogene* *32*, 5388–5396.
42. Wang, Y., Arvanites, A.C., Davidow, L., Blanchard, J., Lam, K., Yoo, J.W., Coy, S., Rubin, L.L., and McMahon, A.P. (2012). Selective identification of hedgehog pathway antagonists by direct analysis of smoothened ciliary translocation. *ACS Chem. Biol.* *7*, 1040–1048.
43. Wang, Y., Zhou, Z., Walsh, C.T., and McMahon, A.P. (2009). Selective translocation of intracellular Smoothened to the primary cilium in response to Hedgehog pathway modulation. *Proc. Natl. Acad. Sci. USA* *106*, 2623–2628.
44. Lim, J., Li, X., Yuan, X., Yang, S., Han, L., and Yang, S. (2020). Primary cilia control cell alignment and patterning in bone development via ceramide-PKC ζ - β -catenin signaling. *Commun. Biol.* *3*, 45.
45. Hynes, A.M., Giles, R.H., Srivastava, S., Eley, L., Whitehead, J., Danilenko, M., Raman, S., Slaats, G.G., Colville, J.G., Ajzenberg, H., et al. (2014). Murine Joubert syndrome reveals Hedgehog signaling defects as a potential therapeutic target for nephronophthisis. *Proc. Natl. Acad. Sci. USA* *111*, 9893–9898.
46. Corbit, K.C., Aanstad, P., Singla, V., Norman, A.R., Stainier, D.Y., and Reiter, J.F. (2005). Vertebrate Smoothened functions at the primary cilium. *Nature* *437*, 1018–1021.
47. Kashiwagi, M., Hojo, H., Kitaura, Y., Maeda, Y., Aini, H., Takato, T., Chung, U.I., and Ohba, S. (2016). Local administration of a hedgehog agonist accelerates fracture healing in a mouse model. *Biochem. Biophys. Res. Commun.* *479*, 772–778.
48. Briscoe, J., and Théron, P.P. (2013). The mechanisms of Hedgehog signalling and its roles in development and disease. *Nat. Rev. Mol. Cell Biol.* *14*, 416–429.
49. Yang, W., Wang, J., Moore, D.C., Liang, H., Dooner, M., Wu, Q., Terek, R., Chen, Q., Ehrlich, M.G., Quesenberry, P.J., and Neel, B.G. (2013). Ptpn11 deletion in a novel progenitor causes metachondromatosis by inducing hedgehog signalling. *Nature* *499*, 491–495.
50. Skoda, A.M., Simovic, D., Karin, V., Kardum, V., Vranic, S., and Serman, L. (2018). The role of the Hedgehog signaling pathway in cancer: A comprehensive review. *Bosn. J. Basic Med. Sci.* *18*, 8–20.
51. Campbell, V.T., Nadesan, P., Ali, S.A., Wang, C.Y., Whetstone, H., Poon, R., Wei, Q., Keilty, J., Proctor, J., Wang, L.W., et al. (2014). Hedgehog pathway inhibition in chondrosarcoma using the smoothened inhibitor IPI-926 directly inhibits sarcoma cell growth. *Mol. Cancer Ther.* *13*, 1259–1269.
52. Xiang, W., Jiang, T., Guo, F., Gong, C., Yang, K., Wu, Y., Huang, X., Cheng, W., and Xu, K. (2014). Hedgehog pathway inhibitor-4 suppresses malignant properties of chondrosarcoma cells by disturbing tumor ciliogenesis. *Oncol. Rep.* *32*, 1622–1630.
53. Sun, Y., Guo, W., Ren, T., Liang, W., Zhou, W., Lu, Q., Jiao, G., and Yan, T. (2014). Gli1 inhibition suppressed cell growth and cell cycle progression and induced apoptosis as well as autophagy depending on ERK1/2 activity in human chondrosarcoma cells. *Cell Death Dis.* *5*, e979.
54. Rozeman, L.B., Hameetman, L., Cleton-Jansen, A.M., Taminiau, A.H., Hogendoorn, P.C., and Bovée, J.V. (2005). Absence of IHH and retention of PTHrP signalling in enchondromas and central chondrosarcomas. *J. Pathol.* *205*, 476–482.
55. Madisen, L., Zwingman, T.A., Sun, S.K., Oh, S.W., Zariwala, H.A., Gu, H., Ng, L.L., Palmiter, R.D., Hawrylycz, M.J., Jones, A.R., et al. (2010). A robust and high-throughput Cre reporting and characterization system for the whole mouse brain. *Nat. Neurosci.* *13*, 133–140.
56. Voehringer, D., Liang, H.E., and Locksley, R.M. (2008). Homeostasis and effector function of lymphopenia-induced “memory-like” T cells in constitutively T cell-depleted mice. *J. Immunol.* *180*, 4742–4753.
57. Yuan, X., and Yang, S. (2015). Deletion of IFT80 Impairs Epiphyseal and Articular Cartilage Formation Due to Disruption of Chondrocyte Differentiation. *PLoS ONE* *10*, e0130618.
58. Li, X., Yang, S., Han, L., Mao, K., and Yang, S. (2020). Ciliary IFT80 is essential for intervertebral disc development and maintenance. *FASEB J.* *34*, 6741–6756.
59. Yuan, X., Cao, J., He, X., Serra, R., Qu, J., Cao, X., and Yang, S. (2016). Ciliary IFT80 balances canonical versus non-canonical hedgehog signalling for osteoblast differentiation. *Nat. Commun.* *7*, 11024.
60. Liu, M., Alharbi, M., Graves, D., and Yang, S. (2020). IFT80 Is Required for Fracture Healing Through Controlling the Regulation of TGF- β Signaling in Chondrocyte Differentiation and Function. *J. Bone Miner. Res.* *35*, 571–582.
61. Jonason, J.H., Hoak, D., and O’Keefe, R.J. (2015). Primary murine growth plate and articular chondrocyte isolation and cell culture. *Methods Mol. Biol.* *1226*, 11–18.
62. Sun, J., Wei, X., Li, S., Sun, C., Wang, C., Li, P., Wei, D.L., and Wei, L. (2018). The Effects of Indian Hedgehog Deletion on Mesenchyme Cells: Inducing Intermediate Cartilage Scaffold Ossification to Cause Growth Plate and Phalange Joint Absence, Short Limb, and Dwarfish Phenotypes. *Stem Cells Dev.* *27*, 1412–1425.
63. Li, Z., Liu, T., Gilmore, A., Gómez, N.M., Fu, C., Lim, J., Yang, S., Mitchell, C.H., Li, Y.P., Oursler, M.J., and Yang, S. (2019). Regulator of G Protein Signaling Protein 12 (Rgs12) Controls Mouse Osteoblast Differentiation via Calcium Channel/Oscillation and G α i-ERK Signaling. *J. Bone Miner. Res.* *34*, 752–764.